International Journal of Theoretical and Applied Research (IJTAR)
ISSN: 2812-5878

Homepage: https://ijtar.journals.ekb.eg

Original article

Effect of Er2O3 incorporation on thermal stability and optical properties of Bi2O3-PbO-B2O3 glass

A. Abd El-maboud[a] N. AlRefaey [a]

[a] *Al Azhar University - Faculty of Science - Physics Department, Cairo, Egypt*

ARTICLE INFO

Received 30/10/2024
Revised 29/12/2024
Accepted 31/12/2024

Keywords

Er_2O_3 - doped oxide glass
X-ray diffraction
Thermal stability
Optical band gap
Photonic materials
Differential scanning calorimetry
Optical properties.

ABSTRACT

The base glass (25 Bi_2O_3–25PbO-50B_2O_3) was doped with x = 0.5, 1, 1.5, and 2 moles% Er_2O_3 respectively. Glasses were prepared using the conventional melt-quenching method. Characterization was conducted using X-ray diffraction (XRD), glass density (GD), molar volume (Vm), differential scanning calorimetry (DSC), and UV-Vis spectroscopy. The XRD revealed the amorphous nature of the glass network, regardless of the Er_2O_3 content. The GD values exhibited non-monotonic behavior with increasing Er_2O_3 content, while the Vm showed a gradual increase. The bonding characteristics of the glasses under study have been calculated to clarify the effect of Er_2O_3 addition on the atomic glass structure. The DSC analysis showed a considerable increase in the Tg value for lower Er_2O_3 content followed by a sharp decrease. This may reflect the instability of the BO/NBO ratio in the glass matrix. In general, doping was found to increase the thermal stability of the glass. The measured optical properties exhibit a non-linear trend; the incorporation of 1.5 mole% of Er_2O_3 resulted in anomalous behaviors as a huge extension of the band tail to inside the forbidden gap occurred. On the other hand, the absorption characteristics revealed that glasses with 0.5 and 2% mole of Er_2O_3 displayed two localized band states inside the energy gap. These findings highlight the potential of Er_2O_3-doped Bi_2O_3-PbO-B_2O_3 glasses for advanced photonic applications.

Graphical abstract

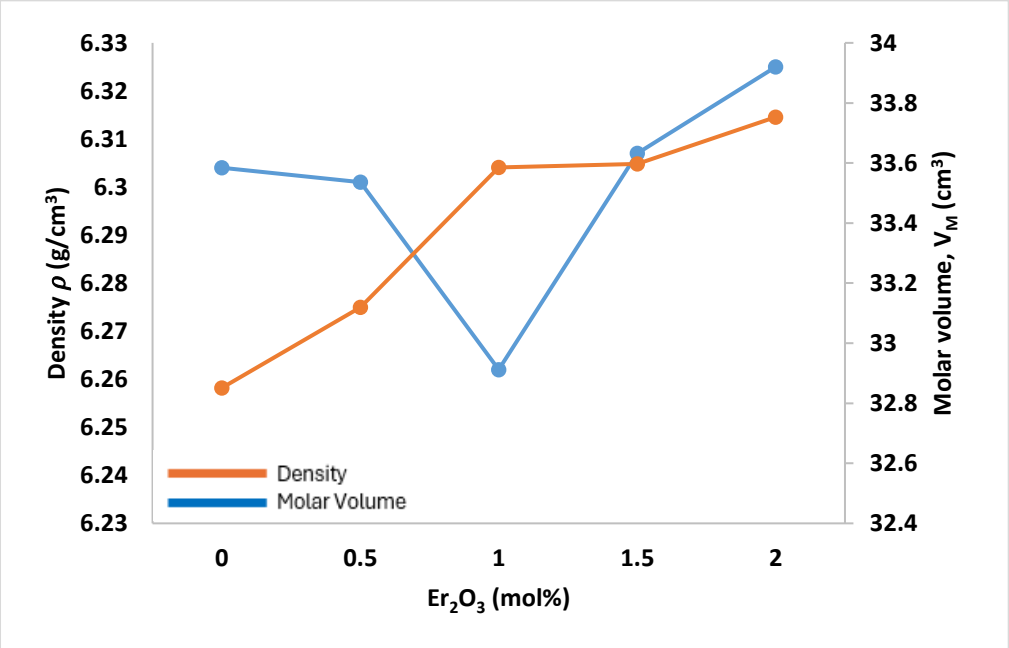

∗ *Corresponding author*
E-mail address: amany@azhar.edu.eg

DOI: 10.21608/IJTAR.2024.331996.1088

1. Introduction

This study aims to investigate the effects of Er_2O_3 incorporation on the thermal stability and optical properties of Bi_2O_3-PbO-B_2O_3 glass. By examining the structural, thermal, and optical behaviors under varying Er_2O_3 concentrations, this research contributes valuable insights for photonic applications and the development of magneto-optical materials.

Recently rare earth oxides doped glasses have received significant attention because of their photonic properties over other glass systems [1-3]. They have potential use in laser hosts, waveguides, and in the field of high-energy physics [4]. Rare-earth ions in multi-component glasses are crucial for designing glass ceramics for photonic applications [5]. Heavy metal-containing glasses, such as PbO and Bi_2O_3 - B_2O_3 , are particularly suitable for non-linear applications. Such ceramic glasses have reduced photon energy-enhancing, thus enhancing the quantum efficiency of photoluminescence emission from excited states of rare-earth ions. [2].

In this study, 'field strength' refers to the electrostatic force around Er^{3+} ions, which is influenced by both the ionic charge and the spacing between the ions. The inter-nuclear distance represents the average spatial separation between Er3+ions within the glass matrix. The terms bonding orbitals (BO) and non-bonding orbitals (NBO) describe the electron configurations within the glass structure: BOs are formed by covalent bonds, while NBOs represent lone pairs or weakly interacting electrons. Finally, RE-O space refers to the separation between rare-earth ions and oxygen atoms, which influences the structural compactness of the glass.

Doping with lanthanides like Er_2O_3 has been shown to influence the thermal stability and optical properties of glass materials [5]. To our knowledge, no previous studies on the effect of Er_2O_3 on Bi_2O_3–PbO-B_2O_3 have been reported. However other studies on the effect of Er_2O_3 incorporation on phase stability have been reported for zirconia [6]. The effect of Er_2O_3 was also investigated to study some elastic and thermal parameters associated with the non-destructive ultrasonic technique [7]. The presence of Er^{3+} ion in phosphate glass was reported to generate 1.54 μm wavelengths which can be utilized for optical amplification [8]. The present work aims to investigate the effect of Er_2O_3 doping on the structural and physical properties of 25 Bi_2O_3–25 PbO–$50B_2O_3$. The density and the molar volume have been investigated and the glass thermal stability was followed through the DSC analysis. Finally, the optical band gap and the associated band tail width were also studied. Abnormal characteristics were detected for different values of Er_2O_3.

2. Material and Methods:

The glass system $25Bi_2O_3$–25Pbo–$50B_2O_3$ doped with 0.5, 1, 1.5, and 2 moles % of Er_2O_3 was prepared via the conventional melt-quenching technique [2]. Batch calculations were performed, and the appropriate amounts of B2O3, PbO, Bi_2O_3, and Er_2O_3 (all with 99% purity) were weighed, The melt was then thoroughly mixed. The batch mixture was transferred into a porcelain crucible and melted in an electric furnace in the temperature range of 1200 °C for 1 h in a normal atmosphere. The melt was then quenched in a pre-heated stainless steel mold to prevent thermal stresses from rapid, uneven cooling.

Philips analytical X-ray diffractometer, type PW3710 based on Cu tube anode was used to test the glass structure, as shown in Figure 1, confirming the amorphous nature of the samples.

The density was measured according to the Archimedes method. For optical measurements, a JASCO-V570 spectrophotometer ($195nm \leq \lambda \leq 2500nm$) was employed. The samples were plate-shaped with a thickness ≈ 2 mm.

3. Results and Discussion

3.1 Density and molar volume

The measured values of density are given in Table 1 and illustrated in Figure 2, and Fig.(7). (The accuracy of the results is $\pm$ 0.001 g/cm^3). The density shows a non-linear trend as a function of Er_2O_3 content. The decrease detected for x = 0.5 and 1 mole% is followed by a further increase up to x = 2 mole%. The experimental values range between 6.301 g/cm^3 for pure glass and 6.325 g/cm^3 for highly doped samples. This non-monotonic behavior suggests structural rearrangements within the glass matrix. At lower concentrations (0.5 mol%), the glass network expands due to disruption caused by Er^{3+} ions, leading to a slight decrease in density and an increase in molar volume, as shown in Figure 2. As the Er_2O_3 content increases, the network reorganizes into a more compact structure, reflected by the gradual increase in density and stabilization of the molar volume. These findings, illustrated in Figure 2, indicate that Er_2O_3 acts as a network modifier, influencing the overall glass compactness. As the density is related to glass compactness, these varying values would suggest that some structure rearrangement has occurred in the glass network with Er_2O_3 incorporation.

The decrease in density observed at 0.5 mol% Er_2O_3 can be attributed to an initial expansion of the glass network as Er3+ ions disrupt the compactness of the existing structure. This expansion increases the inter-nuclear distance and rare-earth ion separation. As the doping level increases beyond 1.5 mol%, a higher Er_2O_3 concentration leads to reorganization within the glass matrix, including the formation of tighter local clusters, resulting in decreased inter-nuclear distances and increased density. This behavior aligns with trends observed in similar heavy-metal borate glasses, where dopant ions act as network modifiers [21-23].

This observed behavior can be explained by the dual role of Er_2O_3 in the glass matrix. At lower concentrations, Er_2O_3 acts as a network modifier, introducing localized structural disorder by disrupting the glass network and increasing the separation between rare-earth ions. At higher concentrations, Er_2O_3 promotes the formation of tighter clusters, enhancing cross-linking and stabilization within the glass network, which leads to reduced inter-nuclear distances and increased density.

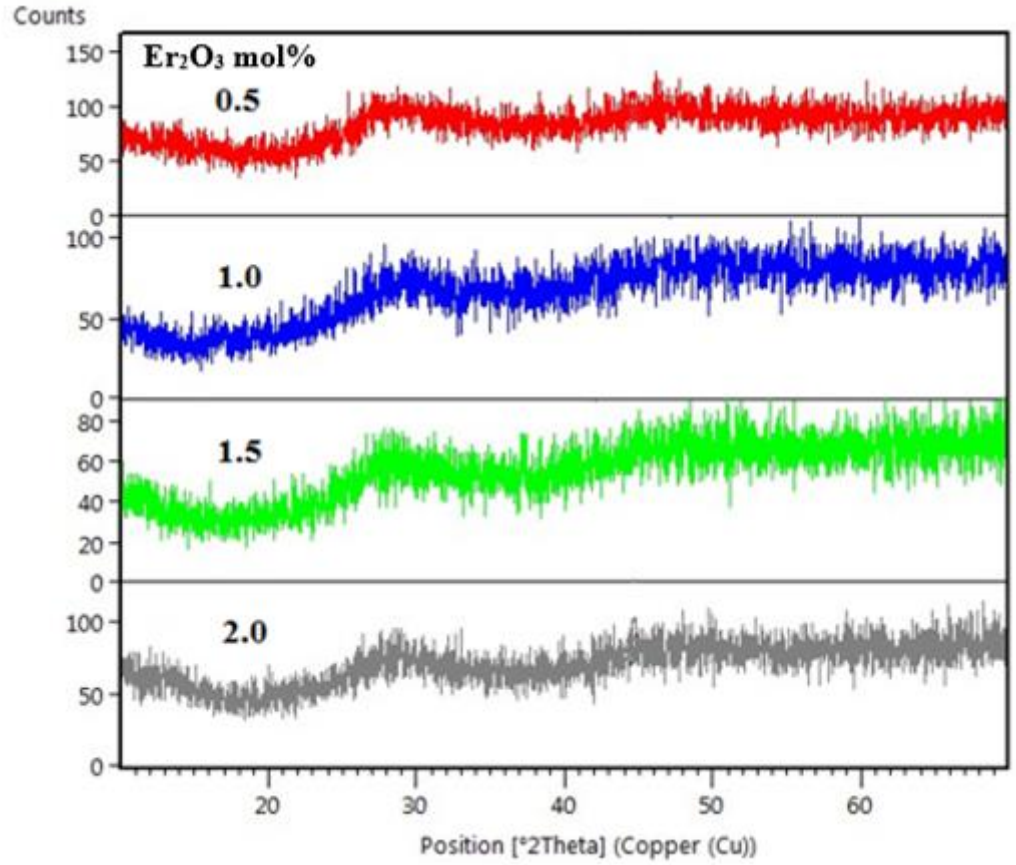

Fig (1). X-ray diffraction patterns of Bi_2O_3-PbO-B_2O_3 glass doped with varying concentrations of Er_2O_3, confirming the amorphous nature of the glass samples

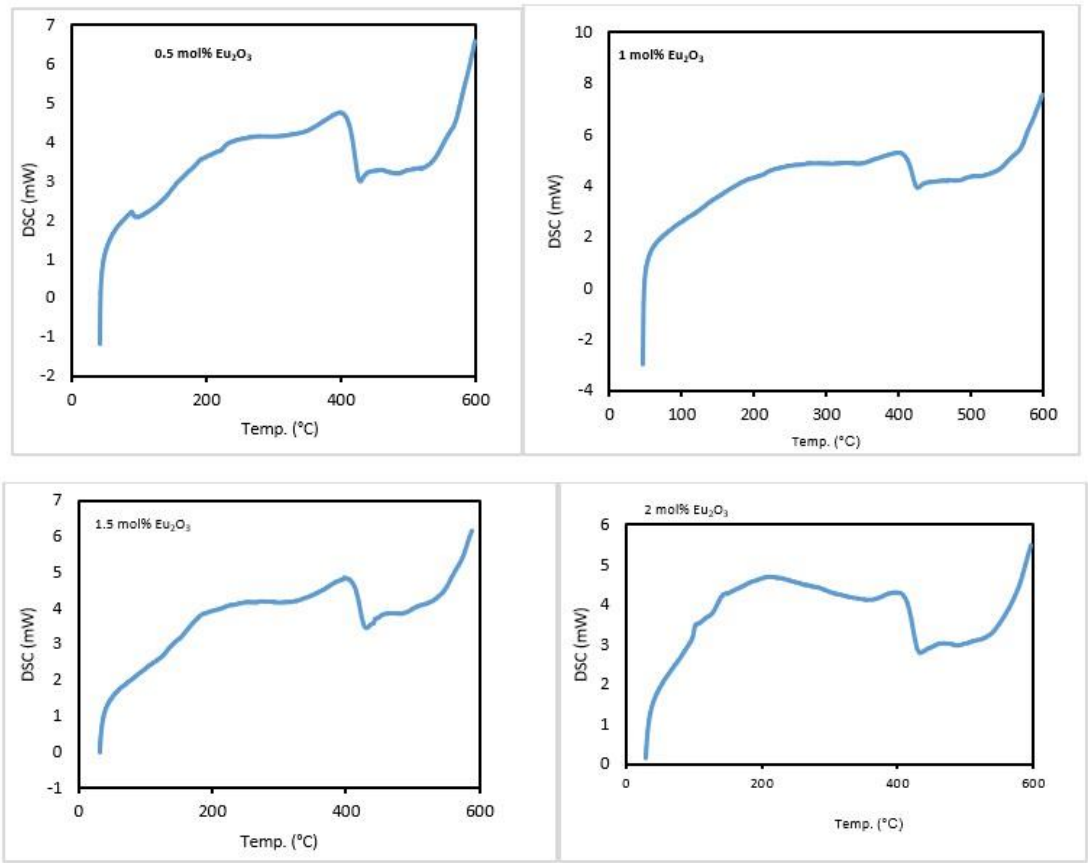

Fig (2). The base glass (25 Bi_2O_3–25PbO-50B_2O_3) was doped with X = 0.5, 1, 1.5, and 2 moles % Er_2O_3 respectively.

Table 1. The density and molar volume of Er_2O_3 doping in Lead bismuth borate glasses.

Er_2O_3 mol%	Density ρ (g/cm^3)	Molar volume (cm^3)
0	6.304	32.851
0.5	6.301	33.119
1	6.262	33.585
1.5	6.307	33.597
2	6.325	33.753

The molar volume has been calculated following the relation [9]:

$$Vm = \frac{\sum_{i=1}^{n} x_i m_i}{\rho} (\text{cm}^3/\text{mole}) \qquad (1)$$

Where x is the molar fraction, m is the weight of each component (i), n is the number of components in the mixture and ρ is the measured density. The molar volume shows an increment trend with increasing the dopant content.

Although the density and molar volume show usually opposite behavior, the present study confirms that the molecular weight is the controller parameter in the monotonically increasing Vm. Other borate glass systems also reported similar behaviors [10, 11].

In the table (2) and figures (2, 3) calculated values of Er^{+3} ion concentration (N), the rare earth ion separation (r_p), the inter-nuclear distance (r_i), and the field strength F around Er ion are given as a function of Er_2O_3 content. These parameters are calculated according to the equation [2]:

$$N = \frac{\rho \, Avogadro\ No\ (Er_2o_3\ mol\%)}{Glass\ average\ molecular\ weight}$$

$$r_i(\text{Å}) = \left(\frac{1}{N}\right)^{\frac{1}{3}}$$

$$r_p(\text{Å}) = \frac{1}{2}\left(\frac{\pi}{6N}\right)^{\frac{1}{3}} \qquad (2)$$

$F = \frac{z}{r_p^2}$, where z is the valence of Er ion.

Here, field strength (F) is calculated using the relation $F = \frac{Z}{r_p^2}$, where z is the ionic charge and r_p is the rare-earth ion separation. The field strength provides insights into the electrostatic interactions around the Er^{3+} ions, which influence the structural properties of the glass matrix.

Increasing N is accompanied by a gradual decrease of both the rare-earth ion separation and the inter-nuclear distance, as shown in Figure 3. Table 2 and Figure 3 also indicate that the incorporation of Er_2O_3 in the glass network greatly increases the lattice field strength. This result is expected as reducing the average RE– ions spacing would increase the field strength around the Er^{3+} ion [13].

3.2. Thermal stability

The measured values of the glass transition temperature (Tg), the onset of crystallization (Tc), the peak value of crystallization (T_l), and the melting point (T_M) are displayed in Table 3. The calculated parameter $\Delta T = (T_c - T_g)$ is also given.

As shown in Table 3, the values of Tg decreased as the Er_2O_3 content increased. The decrease in Tg values with higher Er_2O_3 content suggests a reduction in network rigidity, likely due to increased non-bridging oxygen (NBO) density. At lower doping levels, the increased non-bridging oxygen (NBO) density causes localized disruptions in the glass matrix, leading to a reduction in network rigidity. However, With higher Er_2O_3 content, NBO units promote the formation of stronger local bonding structures, which enhance cross-linking and improve the glass's overall thermal stability. This dual effect explains the observed trends in ΔT values and aligns with the role of Er_2O_3 as a network modifier and stabilizer, as presented in Table 3. However, the remarkable increase of ΔT from 170 to 260 as x increases from 0.5 mole % to 2.0 mole % indicates enhanced cross-linking and stabilization of the glass structure at higher Er_2O_3 levels.

These trends highlight the dual role of Er_2O_3 as both a disruptor and a stabilizer, depending on its concentration. This seemingly contradictory behavior reflects the dual role of Er_2O_3 as both a network modifier and a network former. At lower concentrations, Er_2O_3 disrupts the network structure by introducing non-bridging oxygen (NBO) units, reducing the overall network rigidity. As the concentration increases, Er_2O_3 acts to enhance cross-linking within the glass matrix by forming stronger local structures and increasing the coordination number of the network, as indicated by the ΔT values in Table 3. Thus, increasing the coordination number of the glassy matrices [14,15]. This is going well with the drop recorded in the r_p value given in Table 2.

The RE-O space refers to the distance between rare-earth ions and oxygen atoms, which directly affects the structural rigidity and field strength of the glass matrix. A reduction in the RE-O space typically indicates stronger ionic interactions and a more compact network structure.

3.3 Optical properties

The absorption coefficient (α) cm^{-1} was calculated using Beer Lambert's law [16].

$$\alpha(\upsilon) = 2.303\frac{A}{d} \qquad (3)$$

Where A is defined by log I_o/I and d is the sample thickness. The absorption coefficient (α\) values were calculated with an estimated uncertainty of ±0.01 cm^{-1}, derived from repeated measurements of the same samples. These uncertainties were incorporated into the graphical plots (Figures 4 and 5) as error bars. Incorporating error estimations ensures that the observed trends, such as the localized states and band tail variations, remain statistically significant and correlate with structural changes in the glass network. Specifically, the absorption broadening observed for 1.5 mol% Er_2O_3 aligns with the higher disorder in the glass matrix, as indicated by the extended error margins in this sample.

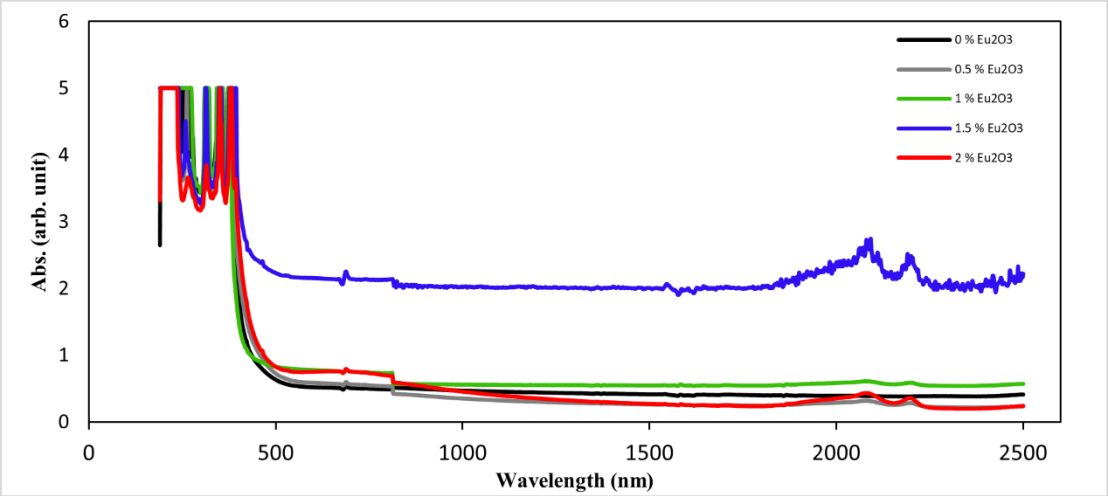

Fig (3)Absorption (arb. unit) of the base glass (25 Bi_2O_3–25PbO-50B_2O_3) was doped with X =0, 0.5, 1, 1.5 and 2 moles % Er_2O_3 respectively.

Table 2. Ion concentration, Field strength, Polaron radius, and inter ionic distance with Er2O3 (mol%) doping in Lead bismuth borate glasses.

Mol % Er_2O_3	Field strength, F (x10^{17} cm^2)	ion concertation, N (x10^{22} ions/ cm^3)	rare earth ion separation r_p (x10^{-8} Å)	inter-nuclear distance r_i (x10^{-8} Å)
0.5	4.5	0.91	1.9	4.79
1	7.2	1.8	1.5	3.82
1.5	9.3	2.7	1.3	3.35
2	11.2	3.5	1.2	3.05

Table (3). Thermal parameters of Er2O3 (mol%) doping in Lead bismuth borate glasses.

Er_2O_3 mol% / DSC Parameter	Er_2O_3 mol% 0	Er_2O_3 0.5 mol%	Er_2O_3 1 mol%	Er_2O_3 mol% 1.5	Er_2O_3 2mol%
Melting temperature T_M (C^0)	485	430	427	431	432
Glass transition Tg (C^0)	208	224	212	183	143
T_l	--	439	437	436	455
T_c	--	394	398	402	403
$\Delta T = (T_c - T_g)$	--	170	186	219	260

Additionally, to better understand the observed behavior in the absorption characteristics and energy gap varia- A closer look at the role of Er_2O_3 in modifying the network structure, particularly at higher doping levels (1.5 and 2 mol%), may reveal how structural disorder impacts the optical absorption properties. Notably, localized states and increased lattice defects (such as oxygen vacancies and broken bonds) contribute significantly to the extension of the absorption tail. This could be crucial for enhancing the efficiency of devices based on these glasses, including photonic and optoelectronic applications. The detailed behavior of localized states within the glass matrix could provide further insight into tailoring optical properties for specific technological purposes.

To calculate the optical band gap width, the Tauc relation is used [17, 18].

$$\propto hv = \beta\,(hv - Eg)^n \qquad (4)$$

tions, further analysis of the disorder-induced localized states inside the forbidden gap is necessary.

Where β is a constant and n is a parameter related to the type of optical transition n = 2 is found to give the best fitting of the plat $(\alpha hv)^{1/2}$ versus hv as shown in Fig. (7). The optical band gap (Eg) is determined from the intersection of the straight line of the plot with the X-axis.

In table 4., we display the calculated Eg for each Er_2O_3 content. Generally, there is a monotonic decrease of the optical band gap to the pure glass except for x = 1 mole % where an increase of 0.08 eV is detected. The bond cohesive energy is known to be proportionally related to the Eg value, hence the decrease detected for Eg with increasing Er_2O_3 content may be attributed to a decrease of bridge oxygen (BO) units where the electrons are strongly bonded. This is more remarkable for the glass with 1.5 mole % of Er_2O_2. A non-monotonic increase of

Eg values was reported for phosphate glasses doped with Er_2O_3 [8], while other workers detected monotonic behaviors of Eg in tellurite oxide [19].

In ideal crystalline materials, no absorption is expected below the energy band gap edge, so a steeply rising absorption edge is detected. In glassy materials, one finds an exponentially increasing absorption edge. This is known as Urbach's rule [20]:

$$\alpha(cm^{-1}) = \alpha_o \exp \frac{h\upsilon}{E_a} \qquad (5)$$

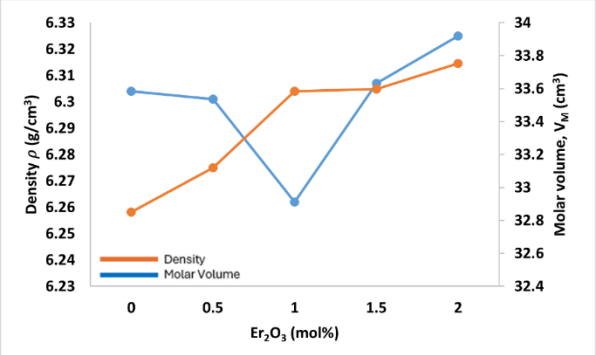

Fig. 4. Variation of the Density and Molar Volume with Er_2O_3 content.

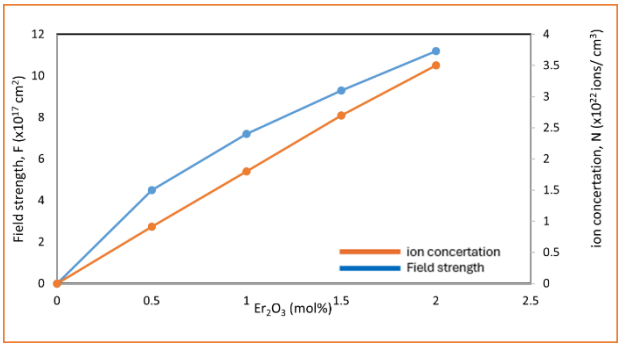

Fig. 5. Variation of ion concentration and field strength with Er_2O_3.

Where Ea is an empirical parameter having the dimension of energy. Plots of ln α $(cm)^{-1}$ against $h\upsilon$ (eV) are given in Fig. (8). As shown, the experimentally determined absorption edge fits an exponential dependency of hυ. Hence a quantity of Ea can be obtained for all Er_2O_3 contents. The energy extension and the absorption intensity are strictly related to the distribution and density of localized states (LSs) inside the forbidden gap. These LSs are created by defects and disorders in the glassy matrix. The noticeably wider energy band gap is associated with narrower band tail width (2.97 eV and 0.15 eV respectively for Eg and Ea for 0.0 mole % and 3.05 eV and 0.14 eV respectively for 1 mole % of Er_2O_3. It seems that the latter is the best to enhance the construction of a chemically ordered amorphous network. Glasses with 0.5, 1.5, and 2 moles % show more than one absorption band inside the forbidden gap (Fig .5). The most pronounced absorption features are observed in the 1.5 mole % dopant sample, indicating increased structural disorder. More lattice disorders and defects (O vacancies, broken bonds, NBO, etc…) are more concentrated in this glass network.

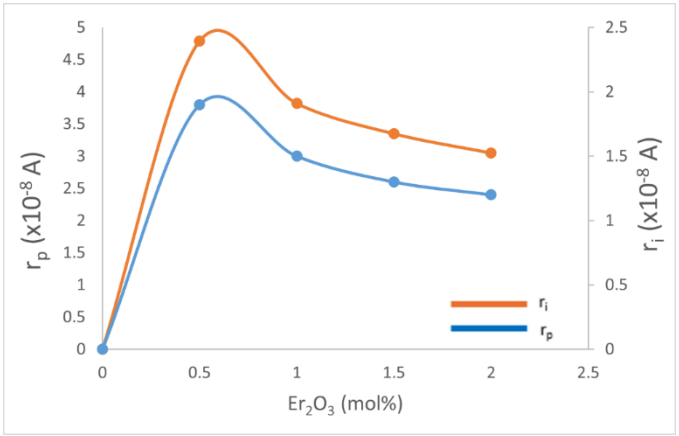

Fig. 6. Variation of rare earth ion separation (rp) and inter-nuclear distance(ri) with Er_2O_3 content.

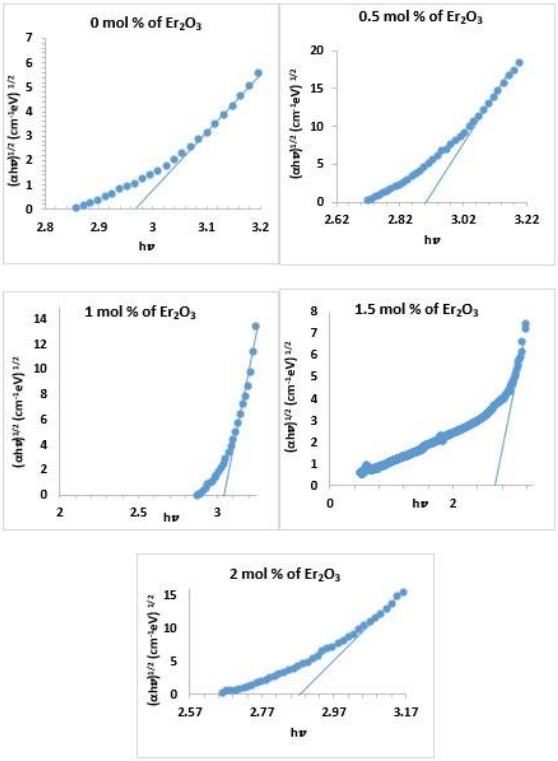

Fig. 7. Variation of (αhν) 1/2 with (hν) for different Er_2O_3 content.

Table (4). Optical Parameters of Eg and Ea for Er_2O_3 (mol%) doping in Lead bismuth borate glasses.

Mol %	Eg $(\alpha h\upsilon)^{1/2}$	Ea (ev)
0	2.97	0.15
0.5	2.86	0.11 & 0.26
1	3.05	0.14
1.5	2.7	0.6 & 2.3
2	2.82	0.3 & 0.13

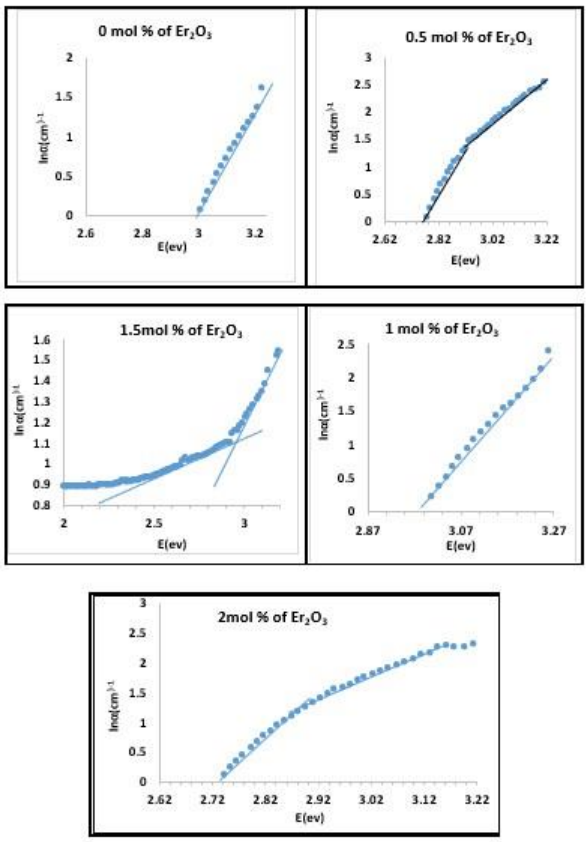

Fig. 8. Variation of (lnα) with (hν) for different Er_2O_3 content.

4. Conclusion

Er_2O_3 doped $25Bi_2O$-25Pb-$50B_2O_3$ glassy system has been prepared by the conventional melt-quenching method. X-ray diffraction analysis confirmed the amorphous nature of all glasses. The XRD patterns, shown in Figure 1, exhibit broad peaks without sharp diffraction peaks, reinforcing the absence of long-range crystallinity and confirming the amorphous state of the glass samples. This structural characteristic is essential for maintaining the desired optical and thermal properties. Retaining the amorphous nature ensures the uniform distribution of Er_2O_3 within the glass matrix, which is critical for photonic and magneto-optical applications.
The measured density shows non-monotonic behavior with increasing Er_2O_3 content, while the molar volume exhibits a gradual increase. Investigation of the glass atomic structure declares the reduction of the RE-O space which-in turn-causes more field strength around the Er^{3+} ion. DSC measurements reveal the effect of Er_2O_3 incorporation on the degree of cross-linkage in the glass network. The Tg values show a wavy trend with increasing dopant content. In general, increasing thermal glass stability is recorded.

The results from XRD, DSC, and UV-Vis spectroscopy offer a detailed understanding of how Er_2O_3 doping influences the structural, thermal, and optical properties, demonstrating the potential of these glasses in advanced photonic applications. These methods effectively capture the trends in density, thermal stability, and optical band gap, aligning with the study's primary objectives.

The optical energy gap exhibits a non-monotonic variation, which has significant implications for tailoring the properties of these glasses for specific photonic and optoelectronic applications. Wider Eg is recorded for sample with x =1 mole % (3.05 eV) while the smallest gap was calculated for x = 1.5 mole % (2.7 eV). The non-monotonic variation in Eg values reflects changes in the bonding environment, specifically the ratio of bonding orbitals (BO) to non-bonding orbitals (NBO). The smallest Eg value at 1.5 mol% suggests the highest degree of structural disorder, consistent with the presence of more localized states in the band gap. Conversely, the sample with 1 mol% Er_2O_3 shows the widest Eg, indicating a more chemically ordered amorphous network. This may be attributed to the percentage of BO to NBO in the glassy matrix.

Absorption band tail plots reveal that more than one absorption band exists in the forbidden gap with x = 0.5, 1.5, and 2 moles %. However, the high density and the more extended localized states were detected for 1.5 mol % of Er_2O_3. i.e., more lattice disorder and defects such as O vacancies, broken bonds, and NBO are more accentuated in this glass.

This study demonstrated that a chemically ordered amorphous network is obtained in glass doped with 1 mol% Er_2O_3. Further studies on photoluminescence and laser emission in heavy metal oxide glass doped with 1 mole% of $Er_{2}o_3$ are followed.

References

1. R. Zhang, S. Yang, J. Li, H. Yan, J. Sha, Advantage Engineering Materials, 2021, 2101045, 1. https://doi.org/10.1002/adem.202101045
2. A. Ratep, I. Kashif, J. Mat. Sci: Mater Electronic, 2021, 32: 12340. https://doi.org/10.1007/s10854-021-05865-y
3. G. M. S. Farouk, S. Y. Marzouk, I. S. Mahmoud, M. Ben Henda, M. Afifi, M. A. Abdel-Aziz, M. Alhabradi, Jmrbt, 2020, 7252. https://doi.org/10.1016/j.jmrt.2020.04.086
4. S. Brabi, C. Mugoni, M. Montorsi, M. Affatigato, C. Gatto, C. Siligardi, Version of record: https://www.sciencedirect.com., https://doi.org/10.1016/j.jnoncrysol.2018.07.033
5. M. Sroda, J. Therm. Anal. Calorim., 2009, 97, 239. https://doi.org/10.1007/s10973-009-0257-3
6. S. L. Tekeli, B. Akatas, M. Kucuktuvek, 3rd Int. Conf., Univ. College of Engineering Tehran, Iran, 2-3 Nov. 2011. https://doi.org/10.1515/htmp-2011-0145
7. U. S. A. Umar, M. K. Halimah, M. N. Azlan, L. U. Grema, Sciences, Springer Nature AC, 2020, 2, 291. https://doi.org/10.1007/s42452-020-2112-x
8. S. M. R. Sahar, K. Z. Lshak, N. A. Sazali, E. S. Yusoff, Research & Reviews: J. Pure Appl. Phys., 2015, 3, 3, 18. https://doi.org/10.4028/www.scientific.net/msf.846.149
9. F. El-Diasty, A. A. Wabav, J. Appl. Phys., 2006, 100, 093511-1. https://doi.org/10.1063/1.2362926

10. S. N. Mohamed, A. K. Yahya, Ionics (Kiel), 2017, 1. https://doi.org/10.1007/s11581-017-1973-5
11. A. M. Abdelghany, A. H. Hammad, Spectrochim. Acta-Part A, 2015, 137, 39. https://doi.org/10.1016/j.saa.2014.08.012
12. A. S. Rao, Y. N. Ahammed, R. R. Reddy, Opt. Mater., 1998, 10, 245. https://doi.org/10.1016/s0925-3467(97)00055-4
13. M. F. Samir, A. F. Metawe, M. Elokr, J. Non-cryst. Sol., 2013, 14-21, 321. https://doi.org/10.1016/j.jnoncrysol.2013.04.001
14. S. Subhadra, S. Sanghi, A. Agarwa, V. P. Sefh, N. Kishove, Mater. Chem. Plup., 2005, 90, 83. https://doi.org/10.1007/s10853-005-0654-3
15. B. Kim, E. Lion, J. Lee, J. Kim, Eur. Ceram. Soc., 2007, 27, 819. https://doi.org/10.1016/j.jeurceramsoc.2006.04.013
16. S. Mohan, K. S. Tined, G. Sharmo, J. Phys., 2007, 37, 4. DOI not found.
17. N. E. Mott, E. A. Davis, Electronic Processes in Non-Crystalline Materials, Oxford, 1979. https://doi.org/10.1515/9783112653326-018
18. E. A. Davis, N. E. Mott, Phil. Mag., 1970, 22, 179, 903. https://doi.org/10.1080/14786437008221061
19. H. J. Sidek, R. El. Malaway, S. Shawaliza Badaron, H. Kamari, K. Matori, Advances in Mater. Sci. and Engin., 2015, Article ID: 628954. https://doi.org/10.1155/2015/628954
20. J. I. Pankove, Optical Processes in Semiconductors, Dover Publications Inc., New York, 1971. https://doi.org/10.1149/1.2404256
21. R. K. Brow, 'The structure of simple phosphate glasses,' J. Non-Cryst. Solids, 1998, 223, 233-241. https://doi.org/10.1016/s0022-3093(99)00620-1
22. A. B. Seddon, 'Structure and vibrational spectroscopy of heavy metal oxide glasses,' J. Non-Cryst. Solids, 1995, 184, 44-50. https://doi.org/10.1016/0022-3093(94)00686-5
23. T. Narayana, S. K. Anupama, K. S. Shashank, 'Spectroscopic properties of rare-earth doped heavy metal borate glasses,' Mater. Chem. Phys., 2015, 151, 114-121.